Optimal Photovoltaic Array Configuration Under Gaussian Laser Beam Condition for Wireless Power Transmission

Weiyang Zhou and Ke Jin, *Member, IEEE*

***Abstract*—The high-intensity laser power beaming (HILPB) system is one of the most promising systems in the long-range wireless power transfer field. In the HILPB system, the conversion efficiency at the photovoltaic (PV) receiver will limit the performance of an implemented system. One of the major factors that contribute to the reduction of PV power is Gaussian laser beam. Different PV configurations can be used to reduce the losses caused by Gaussian laser beam. In this paper, an optimal PV array configuration search mechanism for arbitrarily sized PV arrays to enhance the PV power under Gaussian laser beam condition is proposed. In order to do so, the irradiance profile of the Gaussian laser beam is mathematically modeled, which plays an important role in modeling the PV arrays and designing the optimal configuration research algorithms. The corresponding optimal configuration research algorithms for different PV array architectures are proposed so as to maximize the PV array output power under Gaussian laser beam condition. All the possible optimal solutions for different architectures are compared with each other to find out which one maximizes output power by means of simulations and experiments. The experimental and simulation results are shown to verify the proposed search mechanism.**

***Index Terms*—Array configuration, Gaussian laser beam, maximum power point (MPP), nonuniform irradiance, photovoltaic (PV), wireless power transmission.**

I. Introduction

IN RECENT years, there has been a boom in the development of wireless power technology [1]. Normally, wireless power systems fall into two main categories: short range, which has a typical transmission distance from a few millimeters to a few centimeters, and medium to long range, where the coverage is greater or equal to a typical personal area network [2]. Nowadays, short-range wireless power transfer has found applications in everyday life, such as wireless charging of consumer electronics and biomedical implanted devices [3], [4], while the concept of a long-range wireless power transmission system has been ahead of its practical implementation for a long time, but this gap is shrinking. The high-intensity laser power beaming (HILPB) system is an enabling long-range wireless power technology [5]. It has the capability to deliver energy indefinitely to remote mobile electronic device, such as unmanned aerial vehicle, robots, and orbiting satellites, with advantage of high power density and flexible device, thereby increasing their coverage and endurance. The vast application potential makes the pursuit of the HILPB system a worthwhile endeavor.

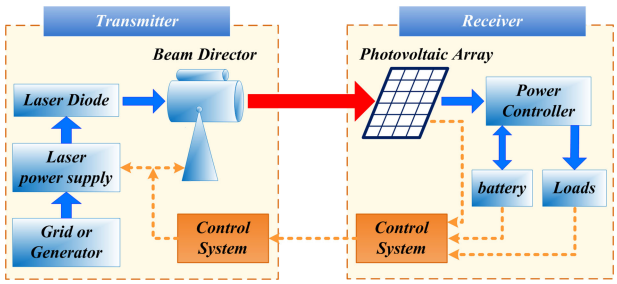

Fig. 1. Schematic diagram of an HILPB system.

Fig. 1 schematically shows the HILPB system. It converts electricity into light via laser diodes (LD), and directs the laser beam to a remote photovoltaic (PV) receiver. The PV array converts the light back into electricity to power the load or charge a battery. Ideally, the HILPB system would have the ability to transmit any amount of power to any point in space, but the conversion efficiencies at the source and the receiver will limit the performance of an implemented system.

A limiting factor in the performance of the PV receiver under HILPB conditions is the energy profile of the incident light. The energy profile across laser beam is Gaussian in nature [6]. Since the very nature of the propagation of a laser beam is not uniform, but fundamentally Gaussian in profile, the PV array is mismatched, leading to undesirable effects such as reduction in generated power and hot pots. Although bypass diodes are used to avoid hot pot damage, the power–voltage ($P-V$) characteristics of the PV array get more complex with multiple peaks. The presence of multiple peaks reduces the effectiveness of the conventional maximum power point tracking (MPPT) schemes leading to the PV array becomes more inefficiency.

To mitigate the effects of the nonuniform irradiance, there are two main approaches that have been proposed. The first group

Manuscript received August 26, 2015; accepted June 9, 2016. Date of publication June 22, 2016; date of current version February 2, 2017. This work was supported in part by the National Natural Science Foundation of China under Grant 51377080, by the Natural Science Foundation for Distinguished Young Scholars of Jiangsu Province (BK20130036), by the Research Fund for the Doctoral Program of Higher Education of China (133218110015), the Nanjing University of Aeronautics and Astronautics Fundamental Research Funds under Grant NE2013102, and by the Six Talents Peak Project of Jiangsu Province 2014-DZXX-017. Recommended for publication by Associate Editor M. Vitelli.

The authors are with the Jiangsu Key-Laboratory of New Energy Generation and Power Conversion, College of Automation Engineering, Nanjing University of Aeronautics and Astronautics, Nanjing 210016, China (e-mail: zwy030710525@163.com; jinke@nuaa.edu.cn).

Color versions of one or more of the figures in this paper are available online at http://ieeexplore.ieee.org.

Digital Object Identifier 10.1109/TPEL.2016.2583502

includes modified MPPT techniques that properly detect the global maximum power point (MPP). Among them, there are power curve slope, load-line MPPT, dividing rectangles techniques, the power increment technique, neural networks, particle swarm optimization, etc., [7], [8]. Obviously, it can harvest more energy by utilizing these MPPT techniques, but it does not prevent the adverse effects of the nonuniform irradiance fundamentally.

An alternate approach is one that employs different PV array configurations for interconnecting PV cells or modules, which are typically either series–parallel (SP), total-cross-tied (TCT), bridge-linked (BL) or honey-comb (HC) configurations, in order to essentially alleviate the nonuniform irradiance effects [9]–[15]. In [9], a modified SP array which is constructed with a highly parallel, rather than serial, wiring configuration is proposed. The highly parallel-configured PV array is capable of making every cell in the panel generate nearly maximum power simultaneously, no matter whether the illumination distribution is uniform. But the output voltage of this modified SP array is low, which makes it difficult to design and optimize an appropriate PV power converter. In [10] and [11], it is found that the interconnections between the PV strings are able to balance the irradiance across each tier in the TCT structure. This may decrease the current that flows through the mismatched cells, thus blocking the operation of bypass diodes. Therefore, compared with the traditional SP array structure, the TCT structure can improve the MPP of the PV array under nonuniform irradiance conditions. In [12]–[16], a reconfigurable PV array is presented. It is noted that the reconfigurable PV array shows the most improvement of MPP compared with the TCT configuration in specific design operating conditions.

What is more, whatever PV array structure is ultimately applied, there will be some form of search algorithms that can be applied to the corresponding array structures to determine the arrays to be configured in ways to improve the power output. In most research studies, the algorithms for TCT architecture have been focused on. In [16], a reconfiguration algorithm for TCT architecture required an offline determination of all possible configurations of the PV array is proposed. Then, the best configuration for the current shading condition was found online. As the number of possible configurations will increase for larger PV arrays and it will be very difficult to find the optimal configuration in a timely manner. It can be concluded that the proposed algorithm in [16] is more suitable for small PV arrays. In order to reduce the computation cost, some quicker real-time reconfiguration algorithms for TCT architecture that determine how to adaptively reconfigure solar cell connections are proposed in [12]. These algorithms are designed to establish near optimum configuration in a very fast time. As to the Gaussian laser beam condition, the PV array faces the constant condition of irradiance environment. Thus, instead of developing the real-time executable algorithms, there is a need to develop the optimal static configuration research algorithms which are suitable for PV array under the Gaussian laser beam condition to establish more optimum configuration within an acceptable time complexity.

In those research works mentioned above, most PV arrays face an unpredictably chaotic irradiance environment. The optimal configuration which is able to maximize the PV array output power under nonuniform illumination conditions is dynamically changed according to the changing nonuniform illumination pattern, while the illumination distribution of the PV array under Gaussian beam condition, which a few works have been focused on, is constant and regular. It is expected that an optimal configuration is existing under the Gaussian laser beam condition. Thus, the development of an optimal PV array configuration search mechanism which improves the PV array performance under the Gaussian laser beam condition will be focused in this paper. The proposed optimal configuration search mechanism finds the optimal configuration based on the improved optimal configuration research algorithms which can be applied to different PV architectures according to the Gaussian distribution of the beam, and all the possible optimal solutions for different architectures are compared with each other to find out which one maximizes the output power.

In this paper, a PV array model, which is able to simulate and analyze the effects of Gaussian laser beam on the output of PV arrays, is proposed in the Section II. An optimal PV array configuration search mechanism which is able to find out the optimal static PV array configuration under the Gaussian laser beam condition is proposed in Section III. The proposed configuration search mechanism is based on the optimal configuration research algorithms that can be applied to existing arbitrary sized array architectures to help optimize the configurations. Finally, the experiment results are shown to verify the effectiveness of the proposed scheme.

II. Model of a PV Array Under Gaussian Laser Beam Condition

The output power of a PV array not only depends on irradiance values of each PV cells, but also depends on other factors such as the interconnection of the individual PV cells, PV cells parameters, and the use of bypass diodes [17]. Thus, the modeling approach will take into account all these factors listed above in this section. The proposed PV model is flexible, interactive, and simple-to-use, which can serve as a simulation tool to study the effect of array configuration on the output power under Gaussian laser beam condition in the next section.

A. Model of a PV Cell

For simulating an entire PV array, the model of a PV cell is developed first. Specifically, the output power of a PV cell strongly depends on the irradiance level of the incident light and ambient temperature. The PV cell equivalent circuit model is shown in Fig. 2 with the current–voltage $(I-V)$ output characteristics are given by [18]

$$I = I_{\rm ph}(G) - I_d(T) - \frac{V + IR_s}{R_p} \tag{1}$$

where

$$I_{\rm ph}(G) = \frac{G}{G_{\rm STC}} \cdot I_{\rm ph}(G_{\rm STC}) \tag{2}$$

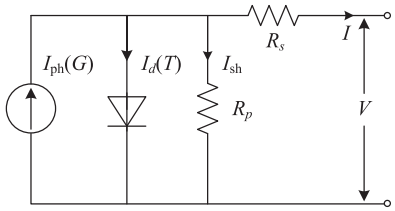

Fig. 2. PV cell equivalent circuit model.

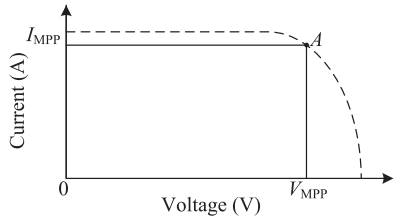

Fig. 3. $I-V$ characteristics of an ideal PV cell.

and

$$I_d(T) = I_o(T)\left\{\exp\left[\frac{q(V+IR_s)}{\mathrm{AkT}}\right]-1\right\}. \tag{3}$$

Parameters in (1)–(3) are defined as follows. G is the irradiance level, T is the cell temperature, q is the charge of the electron, and k is the Boltzmann's constant. STC stands for standard test condition in which the irradiance level is 1000 W/m^2 and the cell temperature is 25 °C.

For the simulation of a real PV cell, the parameters of a PV cell are received by $I-V$ curve fitting approximation from manufacturer's datasheet [19]. These parameters include the following: the photogenerated current at STC $I_{\mathrm{ph}}(G_{\mathrm{STC}})$, PV cell series resistance R_s, PV cell shunt resistance R_p, and diode ideality factor A. The $I-V$ and $P-V$ characteristics of a PV cell at any specific environmental condition (G, T) can be obtained based on this PV cell model by setting the correct value of G and T.

B. Simplified Method for Calculating MPP Power Based on the Ideal PV Model

A simplified method for calculating MPP power which will play an important role in the optimal configuration research algorithm design is introduced first. This method is based on an ideal PV cell model which is proposed in [15], and the following theoretical analysis (espcially the design of the optimal algorithms for the SP and TCT architectures) will be based on this ideal PV cell model. Here, the output voltage, current, and power at MPP of a PV cell/string/array is defined by the MPP voltage, MPP current, and MPP power, respectively.

In reality, the temperature of different PV cells can be differernt due to the effect of Gaussian laser beam. Since the ratio of irradiance between the highest and lowest illuminated PV cells in any PV array under the Gaussian laser beam condition is fixed, in principle, the diffference between temperature of the highest and lowest illuminated PV cells is also fixed as long as these PV cells can withstand the high intensity laser beam. The in-field measurements of 3×3 and 5×5 PV arrays are performed by using the PV system setups with heat sink to provide sufficient thermal dissipation in order to handle the excess unconverted energy, and it is confirmed that a maximum of 10 °C difference between temperature of the highest illuminated PV cell and that of the lowest illuminated PV cell. 10 °C increase in temperature will result in <5% degradation in the MPP power of PV cell according to the model presented in Section II-A.

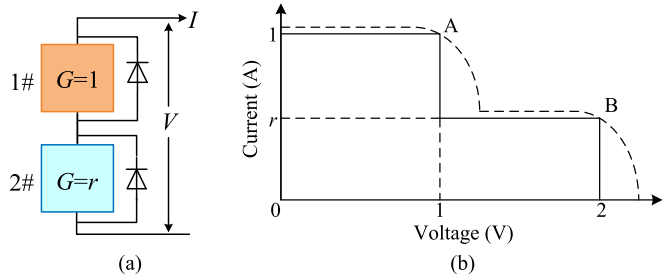

Fig. 4. Example of calculating the MPP power of a single string. (a) Simple PV string. (b) $I-V$ characteristics of an ideal PV string.

Thus, the illumination intensity affects the output power of a PV cell more than the temperature.

As mentioned above, a maximum of 10 °C difference between different PV cells is measured, and 10 °C higher in temperature will also result in <5% degradation in the MPP voltage of PV cell. For simplicity, the impact of temperature on the ideal PV cell can be ignored, that is, the ideal PV cells with different temperature have the same MPP voltage. So the $I-V$ characteristics of an idea PV cell is a step function such that

$$I = \begin{cases} I_{\mathrm{MPP}}, & \text{if} \quad V \le V_{\mathrm{Mpp}} \\ 0, & \text{otherwise} \end{cases} \tag{4}$$

where V_{MPP} and I_{MPP} are the MPP voltage and current of the PV cell, respectively. The constant voltage V_{MPP} is used to approximate the MPP voltage for every PV cell. The current I_{MPP} is largely determined by the cell's photogenerated current $I_{\mathrm{ph}}(G)$, which is linearly dependent on the irradiance G. Fig. 3 schematically shows the $I-V$ characteristics of a real PV cell (the dotted line) and its corresponding ideal PV cell (the solid line).

Based on the idea PV cell assumption, an example of calculating the MPP power of a single string which is shown in Fig. 4(a) is presented. In this figure, the irradiance G, the MPP power, the MPP voltage, and the MPP current of the highest illuminated PV cell 1# are defined as reference value 1, and thus, the values of the MPP power and current of the low illuminated PV cell 2# are both r. The simplified $I-V$ curve of this single string under nonuniform illumination condition is shown in Fig. 4(b), where the solid and dotted line represent the $I-V$ characteristics of an ideal PV string and its corresponding real PV string, respectively. The dot A and B in Fig. 4(b) denote the MPPs of the string, and the power at A and B are 1 and 2r, respectively. If $r > 0.5$, the dot B is the global MPP of the string, and the

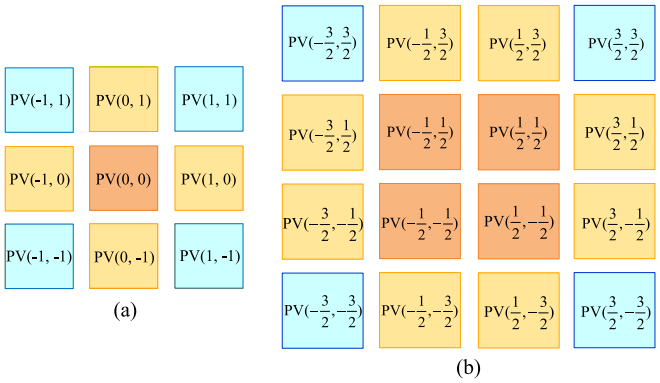

Fig. 5. Cells arrangement in an unconnected PV array. (a) 3×3 PV array. (b) 4×4 PV array.

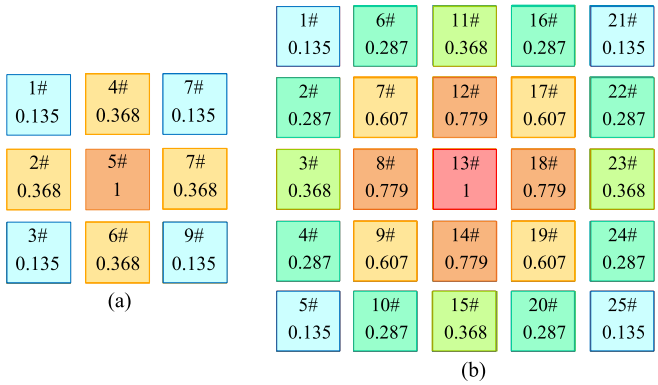

Fig. 6. Irradiance profile model for the 3×3 and 5×5 PV array. (a) 3×3 PV array. (b) 5×5 PV array.

MPP voltage of the string is 2. Otherwise, the dot A is the global MPP, and the MPP voltage of the string is 1.

C. Irradiance Profiling

The laser emits beams that approximate a Gaussian profile. It has nonuniform illumination across the entire PV array, namely the PV cells are illuminated differently. Generally, the PV cells in the center of the array are illuminated by higher irradiation than those in the bounds. The main objective of this paper is to establish a clear relationship between topologies, irradiance profile, and the MPP of the PV array. In order to do so, the characteristics of the simulated irradiance profile must be mathematically modeled. Here, the irradiance profile is a virtual map containing information about a cells physical location and the irradiance across its surface.

In this case, the PV array is modeled as a network with dimension $m \times n$, where m represents the number of PV cells in a column, and n represents the number of PV cells in a row. The 3×3 and 4×4 PV array, as shown in Fig. 5, are used as examples. In this figure, each PV(i, j) is an individual PV cell. The index i, j represents the horizontal and vertical coordinate of the PV cell in this network. It is assumed that the PV cell is relatively small compared with the entire network. The center of the network is defined as position (0, 0), and the distance between the adjoining PV cells is unit 1. Thus, the distance $D_{i,j}$ between the PV cell with index i, j and the center of the network can be defined by the following equation:

$$D_{i,j} = \sqrt{i^2 + j^2}. \tag{5}$$

Realizable values for the normalized irradiance in each PV cell will range from 0 to 1, and can be specified using the following equation, when the irradiance is normalized here [6]:

$$\frac{G_{i,j}}{G_{0,0}} = \exp\left[-\frac{2 \cdot (D_{i,j})^2}{{w_0}^2}\right] \tag{6}$$

where w_0 is the beam radius and can be described using

$$w_0 = \sqrt{\left(\frac{m-1}{2}\right)^2 + \left(\frac{n-1}{2}\right)^2}. \tag{7}$$

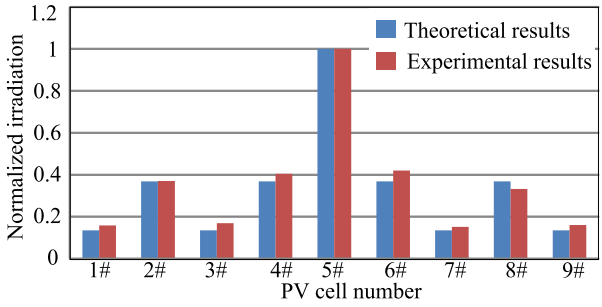

Fig. 7. Comparison between the experimental and theoretical results of the 3×3 PV array.

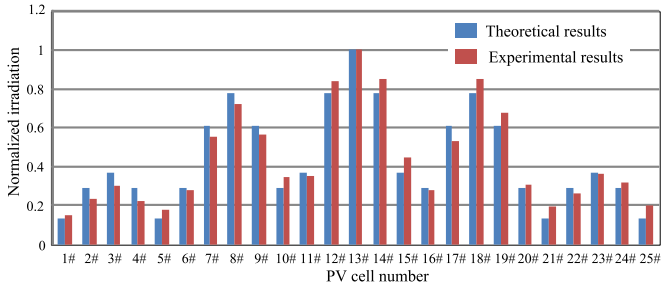

Fig. 8. Comparison between the experimental and theoretical results of the 5×5 PV array.

In general, the three equations above can be used to model the irradiance across a PV array under Gaussian beam condition. Fig. 6 illustrates the calculated normalized irradiation on each numbered PV cell in a 3×3 and 5×5 PV array. As the irradiance is approximately proportional to the short-circuit current so that the short-circuit currents of all the PV cells in 3×3 and 5×5 PV arrays are measured in the experiments in order to verify the validity of the irradiance profile model. The comparisons between the experimental and theoretical results of the normalized irradiation of the PV cells in 3×3 and 5×5 PV arrays are shown in Figs. 7 and 8, respectively. It can be seen from the comparisons that the error between theoretical and measured values is acceptable when considering the factors of the performance difference between the cells and the actual nonstandard

Gaussian laser beam, thus the validity of the irradiance profile model is verified.

The PV array simulation model can be built in the MATLAB or SABER environment. This model is based on the PV cell model described in the Section II-A. The PV array is constructed from the interconnection of PV cells in SP or TCT configuration. It is assumed that each PV cell is integrated with a bypass diode and the blocking diode is connected in series with each of the series strings in this paper. By setting the correct temperture and irradiance on every individual PV cell model in the array, the $I-V$ and $P-V$ characteristics of a PV array which under Gaussian beam condition can be predicted and the effect on different array configurations for a specific irradiance profile can be observed.

III. Optimal PV Array Configuration

In order to cope better with Gaussian beam condition, an optimal PV array configuration search mechanism is proposed in this section. The optimization study explores all available topologies of any given PV array to find out which one maximizes the output power. In order to do so, the optimal configuration research algorithms for different architectures are presented. These algorithms proposed in this paper are iterative and hierarchical sorting algorithms that are designed to provide an optimum solution in an acceptable search time.

A. Different Architectures of PV Arrays

In principle, the output power of the PV array is determined by the power level of the HILPB system, namely, the size of the PV array is fixed for a specific HILPB system. A PV array consisting of Q PV cells may include an arbitrary number (less than or equal to Q) of rows. The number of rows determines the output voltage of the array which affects the efficiency of the power converter that connected at the output of the array. Usually, a step-up power converter is used to manage the array loading and boost the voltage to the system. The power dissipation of the converter is minimized when the output voltage of the PV array is high enough and close to the output voltage of the converter. However, it is preferred to connect all cells in parallel so that the PV array can achieve better performance, which limits the output voltage of the array to be improved. Thus, the output voltage of the PV array $V_{\rm pv}$ needs to be predesigned based on the consideration of the power level of the system, the output voltage and efficiency of the set-up converter, etc. In other word, the voltage $V_{\rm pv}$ will be known in advance before the PV array is designed, and the optimal number of rows *m* in the PV array can be determined according to the voltage $V_{\rm pv}$. For simplicity, it is assumed that the number of rows *m* is fixed for a specific HILPB system in this paper (the voltage $V_{\rm pv}$ is equal to $mV_{\rm MPP}$).

For a PV array with a specific number of cells and rows, the physical layout and the configuration of it are independent of one another. The physical layout of the PV array is an $m' \times n'$ array on a panel, where there are m' rows and n' columns of PV cells. The configuration of the PV array is the actual electrical connection of PV cells in the PV array. Usually, the PV array can be interconnected in a fixed architecture, such as the SP, TCT, BL, and HC architectures. As the Gaussian distribution of the laser beam is fixed and invariable, appropriate design of a PV array configuration can significantly improve the overall system performance to counter the Gaussian laser beam. It is found that the BL and HC architectures are derived from the TCT architecture and they have poorer performance than the TCT and SP architectures [10]. So this paper will focus on the SP and TCT architectures, as shown in Figs. 9 and 10, to explore their performance under Gaussian beam condition.

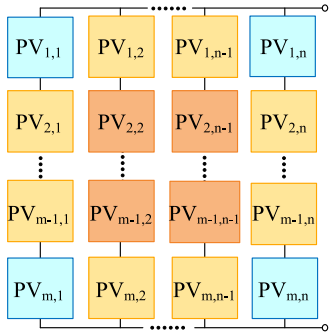

Fig. 9. $m \times n$ SP architecture.

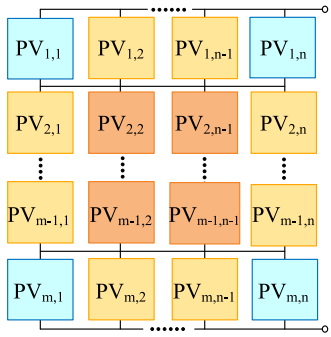

Fig. 10. $m \times n$ TCT architecture.

Obviously, for the SP and TCT architectures, swapping the cells from one position to another can obtain different MPPs. For optimal performance, the optimization algorithms for SP and TCT architectures are proposed to find the corresponding maximum MPPs under Gaussian beam condition. By comparing the maximum MPPs of the SP and TCT configurations, the better configuration can be found out.

B. Optimal SP Configuration Research Algorithm

For an $m \times n$ SP architecture as shown in Fig. 9, there are *n* strings connected in parallel, and each string consists of *m* PV cells in series. The configuration of the *k*th string is defined as $C_k(\mathrm{PV}_{1,k}, \mathrm{PV}_{2,k}, \ldots, \mathrm{PV}_{m-1,k}, \mathrm{PV}_{m,k})$. Let $V_{\mathrm{MPP},k}(C_k)$ and $P_{\mathrm{MPP},k}(C_k)$ represent the MPP voltage and power values, respectively, of the *k*th PV string with a configuration $C_k(\mathrm{PV}_{1,k}, \mathrm{PV}_{2,k}, \ldots, \mathrm{PV}_{m-1,k}, \mathrm{PV}_{m,k})$. As has been discussed previously in this paper, there are a few works that have been focused on the search algorithms for SP architecture. In this paper, the optimal SP configuration search algortithm that

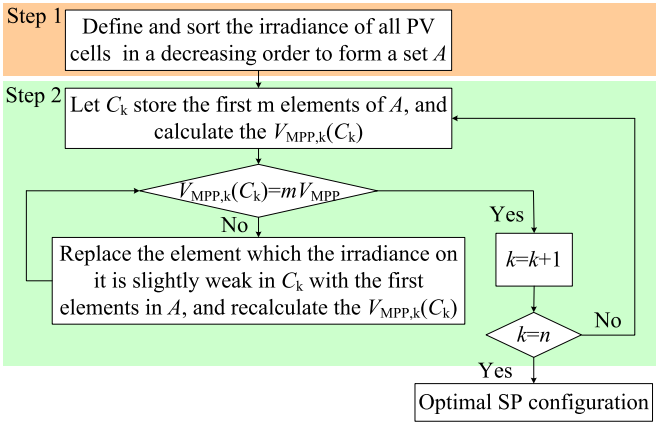

Fig. 11. Flowchart of the algorithm for the SP architecture.

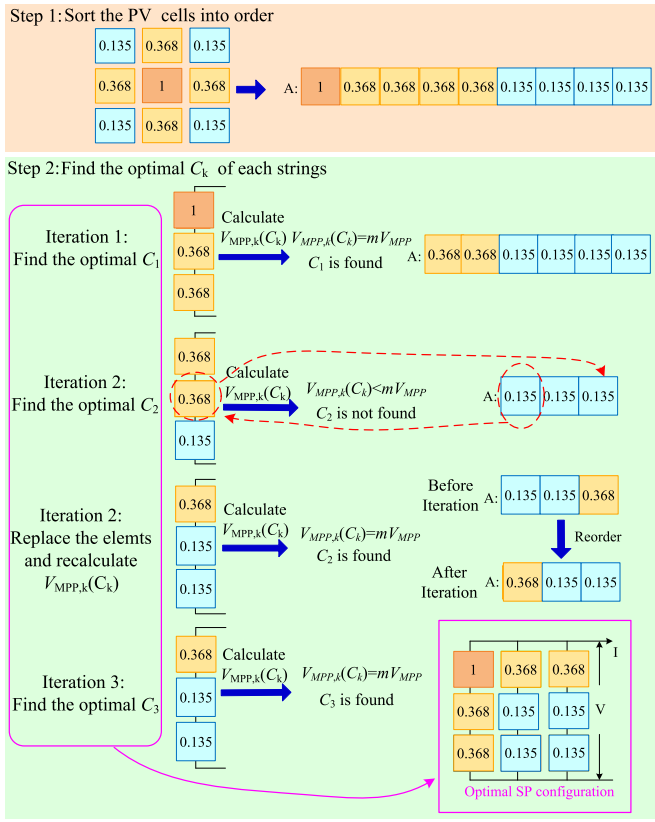

Fig. 12. Example algorithm routine for SP configuration.

borrows the concept of greedy method to establish the optimum configuration is proposed.

For the SP architectures with a specific number of rows m, different SP configurations may have different MPP voltages. The setup converter used for MPPT is generally designed to operate with high efficiency at the voltage mV_{MPP}. However, the efficiency of the setup converter varies with the output voltage of the array, and the MPP of the load when the converter efficiency is considered is different from the MPP of the PV array. Since the maximization of power in the load is ultimately desirable, the MPP voltage of the PV array or the kth PV string needs to be equal to mV_{MPP} to obtain the maximum efficiency energy transfer from the PV array to the load [20].

With the blocking diodes in the PV array, it can be considered that if all strings simultaneously operate at the same MPP voltage, the maximum power harvested by the PV array is the sum of the MPP power of all the PV strings in this array. The algorithm proposed in this paper for the SP architecture aims at finding the optimal $C_k(1 \le k \le n)$ of each string by swapping the cells from one string to another so that the MPP power is maximized for each string with the same MPP voltage. This objective is equivalent to maximize the PV array output power. The flowchart of the algorithm for the SP architecture is shown in Fig. 11. In general, the optimal SP configuration is searched by the following steps:

Step 1: Define and sort the irradiance of all the PV cells in the PV array in a decreasing order and convert to a set A, i.e.,

$$G_{\mathrm{oA}_1} > G_{\mathrm{oA}_2} > \cdots > G_{\mathrm{oA}_j} > \cdots > G_{\mathrm{oA}_{mn}}$$

where G_{0Aj} is the irradiance on the PV cell $A_j(1 \le j \le mn)$. The corresponding PV cell set A can be written in the form

$$A = \{A_1, A_2, \ldots, A_j, \ldots, A_{mn}\}$$

where the elements in A denote the indices of PV cells in the PV array.

Step 2: Find the optimal $C_k(1 \le k \le n)$ of each strings. A greedy algorithm is employed to find an optimal solution in the following principle:

First, in the kth stage, let C_k store the first m elements of A. Correspondingly, the number of elements in set A is reduced to $m(n-k)$. As the irradiances on the PV cells which in the set C_k are closed to each other, it is noted that the $P_{\mathrm{MPP},k}(C_k)$ of kth string is maximized with the configuration C_k at the moment.

Next, calculate the $V_{\mathrm{MPP},k}(C_k)$ using the method in Section II-B. As mentioned above, if $V_{\mathrm{MPP},k}(C_k) = mV_{\mathrm{MPP}}$, it is indicated that this C_k is the optimal configuration for kth string, where mV_{MPP} means that the PV array is set to operate at the output voltage level to the largest possible extent. Otherwise, replace the element which the irradiance on it is slightly weak in C_k with the first element in A. Then recalculate $V_{\mathrm{MPP},k}(C_k)$ and compare it with mV_{MPP}. This process will continue until $V_{\mathrm{MPP},k}(C_k) = mV_{\mathrm{MPP}}$.

The step 2 will continue until all the optimal $C_k(1 \le k \le n)$ are found. Then the optimal SP configuration will be obtained based on these $C_k(1 \le k \le n)$.

A simple example is used to explain the basic idea of this algorithm. Considering the case of a 3×3 array is illuminated under Gaussian beam condition, as shown in Fig. 12. In this figure, the normalized irradiance of each PV cell is labeled inside the PV cell. The algorithm then follows the above steps until the all optimal $C_k(1 \le k \le 3)$ are found. The final configuration which searched by the algorithm is shown in Fig. 12, and the $P-V$ curve of it is numbered 1# in Fig. 13. Fig. 13 shows the $P-V$ curves of all the possible configurations of the 3×3 array by simulation. As seen in this figure, the array 1# outputs the maximum power, which verifies the algorithm.

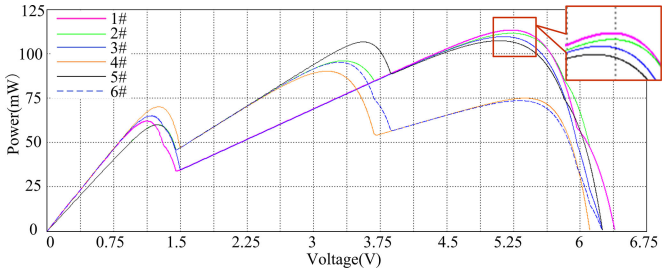

Fig. 13. $P-V$ curves of all possible configurations of the 3×3 SP array.

This method may not guarantee to find the global maximum configuration, but it will produce a configuration that is within an acceptable margin from the optimum. One of the significant advantages of this approach is the simplicity of computation.

C. Optimal TCT Configuration Research Algorithm

For a typical $m \times n$ TCT architecture, as shown in Fig. 10, there are *m* modules connected in series, and each module consists of *n* PV cells in parallel. As has been discussed previously in this paper, most search algorithms for the TCT architecture either be computationally expensive or only provide near optimum solution in a nonuniform irradiance environment, and so, a search algorithm which can provide more optimal solution within an acceptable time complexity under Gaussian beam condition is required. The optimal TCT configuration search algortithm proposed in this paper borrows the concept of irradiance equalization to establish the optimum configuration. Irradiance equalization is the process of swapping the cells from one module to another so that the total irradiance (and therefore current producing ability) at each module is almost equal [12]. Once equalization has been done, a simple way to evaluate the choice of configuration is to subtract the weakest performing module from the best performing module, where the answers closest to zero indicate good equalization.

The flowchart of the algorithm for the TCT architecture is shown in Fig. 14. The algorithm is based on the irradiance equalization method and contains the following steps:

Step 1: Define and sort the irradiance of all the PV cells in the PV array in a decreasing order and converted to a PV cell bank, i.e.,

$$G_{oA_1} > G_{oA_2} > \cdots > G_{oA_j} > \cdots > G_{oA_{\mathrm{mn}}}.$$

Step 2: Connect the cells which stored in the PV cell bank to the corrected module in the TCT configuration.

First, calculate the total irradiance at each module. Then, the total irradiance of all modules of the TCT configuration are sorted in an increasing order, i.e.,

$$G_{M_1} > G_{M_2} > \cdots > G_{M_j} > \cdots > G_{M_m}.$$

Thus, the rows of the TCT configuration and each PV cell have been renumbered according their sorting irradiances.

Next, connect the PV cell with the maximum irradiance of the PV cell bank in parallel to the module which has the smallest

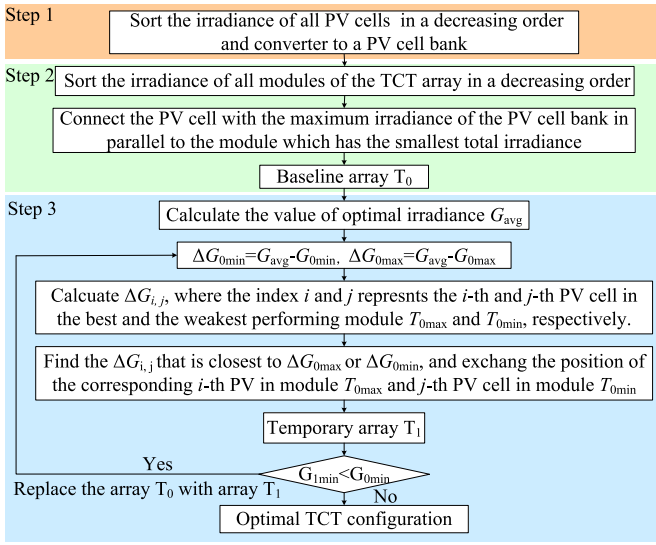

Fig. 14. Flowchart of the algorithm for the TCT architecture.

total irradiance. For example, if PV cell A_1 is connected in parallel with the module in row 1, then after the first iteration, the PV cell bank becomes

$$G_{\mathrm{oA}_2} > G_{\mathrm{oA}_3} > \cdots > G_{\mathrm{oA}_j} > \cdots > G_{\mathrm{oA}_{\mathrm{mn}}}.$$

The total irradiance of the modules in the TCT configuration might become

$$G_{M_2} > G_{M_1} > \cdots > G_{M_j} > \cdots > G_{M_m}.$$

Then the second iteration occurs, and PV cell A_2 is connected in parallel with the module in row 2. This process will continue until all the PV cells of the PV cell bank are connected parallel to the rows of the TCT configuration. Thus, the baseline array T_0 has been done.

Step 3: It is worth noting that the array T_0 is a near optimum solution. There is a need to optimize the configuration of the array T_0 in order to further improve the output power. First, calculate the value of optimal irradiance G_{avg}, and it can be simply found by adding up all of the irradiances and dividing by the number of modules. Therefore, the difference between the optimal irradiance G_{avg} and the total irradiance of the weakest performing module is

$$\Delta G_{0\min} = G_{\mathrm{avg}} - G_{0\min} \tag{8}$$

where $G_{0\min}$ is the total irradiance received by the weakest performing module $T_{0\,\min}$.

Similarly, the difference between the optimal irradiance G_{avg} and the total irradiance of the best performing module is

$$\Delta G_{0\,\max} = |G_{\mathrm{avg}} - G_{0\,\max}| \tag{9}$$

where $G_{0\max}$ is the total irradiance received by the best performing module $T_{0\max}$.

Next, calculate the difference between the irradiance of the *i*th PV cell in module $T_{0\max}$ and the irradiances of the all PV cells, which have lower irradiance value than the *i*th PV cell, in

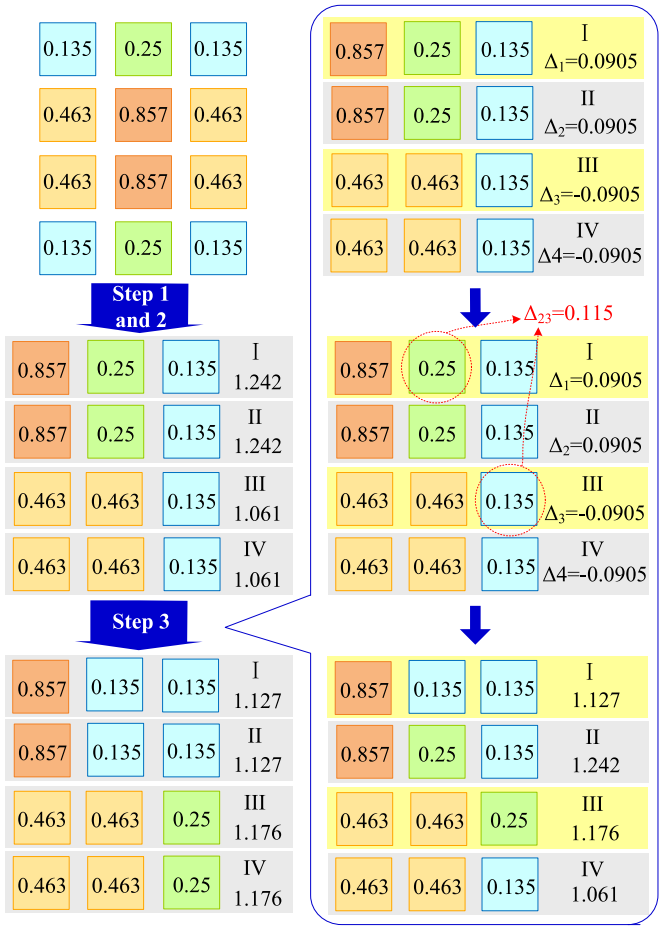

Fig. 15. Example algorithm routine for TCT configuration.

TABLE I
PARAMETERS OF PV CELL

Open-circuit voltage, V_{oc}	2 V
Short-circuit current, I_{sc}	0.04 A
Voltage at MPP, V_{MPP}	1.65 V
Current at MPP, I_{MPP}	0.0349 A
Power at MPP, P_{MPP}	0.058 W

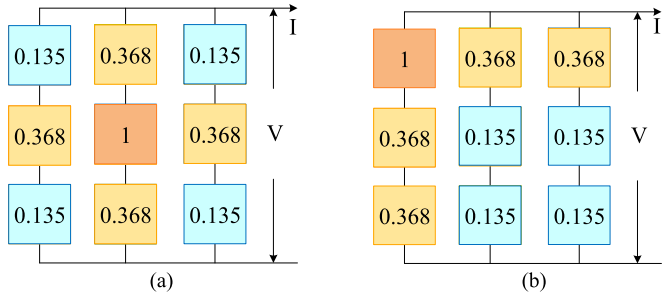

Fig. 16. Optimal configuration for a 3×3 SP PV array. (a) Before the algorithm is executed. (b) After the algorithm is executed.

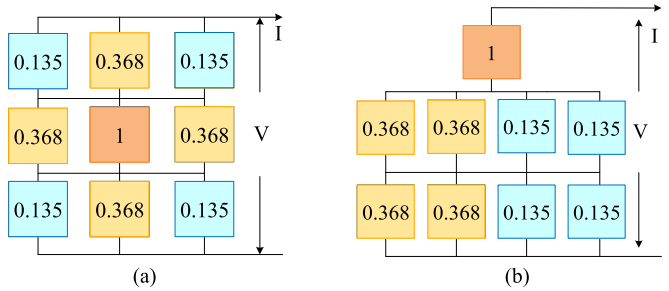

Fig. 17. Optimal configuration for a 3×3 TCT PV array. (a) Before the algorithm is executed. (b) After the algorithm is executed.

module $T_{0\min}$, and the answers are expressed as $\Delta G_{i,j}$, where the index i and j represents the ith and jth PV cell in module $T_{0\max}$ and $T_{0\min}$, respectively. This process will continue until all the PV cells in module $T_{0\max}$ have been traversed.

Then, find the $\Delta G_{i,j}$ that is closest to $\Delta G_{0\max}$ or $\Delta G_{0\min}$, and exchange the position of the corresponding ith PV in module $T_{0\max}$ and jth PV cell in module $T_{0\min}$. Thus, the temporary array T_1 has been done. If $G_{1\min} > G_{0\min}$, where $G_{1\min}$ is the total irradiance received by the weakest performing module in array T_1, it is indicated that the array T_1 has better equalization than array T_0. Therefore, replace the array T_0 with array T_1 and repeat the procedure in Step 3. Otherwise, the array T_0 is the final optimal TCT configuration.

A simple example is used to make the concept of the above algorithm clearer. Consider the case of a 4×3 array is illuminated under Gaussian beam condition, as shown in Fig. 15. In the configurations shown in Fig. 15, the values of the normalized irradiance of the PV cells are labeled inside the PV cells. The algorithm then follows the above steps until final optimal TCT configuration are found. This gives a normalized total irradiance in each row of 1.127, 1.127, 1.176, and 1.176, respectively, and the actual average irradiance of the array is calculated, the average is 1.1515. The errors in each case are, therefore, 0.0245 which are around 2%. This method will produce a configuration that is within an acceptable margin from the optimum. It is efficient and simple.

D. Discussions

A PV array system simulation platform is developed using SABER to verify the proposed algorithms functionality and find out the optimal PV array configuration. In this paper, the detailed models were implemented in the Saber simulator to calculate the detailed circuit level behavior. The specifications of the cell at standard test conditions are shown in Table I and the temperature of the cells is measured in the experiments. In addition to the results presented previously in this paper, the 3×3 and 5×5 PV array under Gaussian beam condition are also simulated considering the temperature effect.

The corresponding optimal configurations for 3×3 SP and TCT PV array under Gaussian beam condition are shown in Figs. 16 and 17, respectively. As seen in Fig. 16, the configuration of the 3×3 SP PV array is not changed before and after the algorithm is executed. It means that the configuration that before the algorithm is executed is already the optimal solution, which has been verified by the results that are shown in

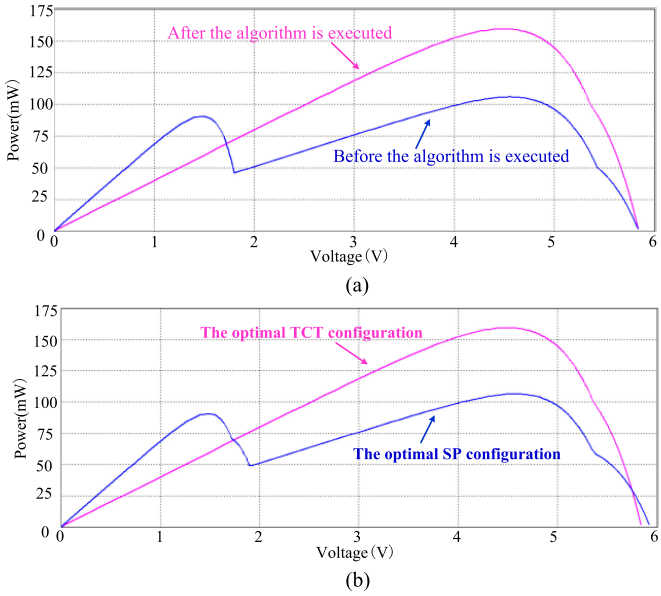

Fig. 18. Simulated $P-V$ curves of a 3×3 PV array. (a) Simulated $P-V$ curves of a 3×3 TCT PV array before and after the algorithm is executed. (b) Simulated $P-V$ curves of the optimal configurations for 3×3 TCT and SP PV arrays.

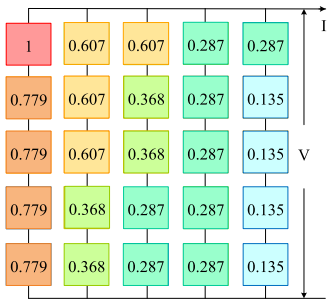

Fig. 19. Optimal configuration for a 5×5 SP PV array.

Fig. 13. The $P-V$ curves for a 3×3 PV array before and after the algorithm is executed are shown in Fig. 18, which assumes that the illumination conditions are the same. As seen in Fig. 18(a), there is a 33% increase in MPP power from before to after the algorithm is executed for the 3×3 TCT PV array. Moreover, as seen in Fig. 18(b), the TCT configuration has better performance than SP configuration with a 33% improvement in MPP power.

The corresponding optimal configurations for a 5×5 SP and TCT PV array under Gaussian beam condition are shown in Figs. 19 and 20, respectively. The $P-V$ curves for a 5×5 PV array before and after the algorithm is executed are shown in Fig. 21, which assumes that the illumination conditions are the same. As seen in Fig. 21(a) and (b), there is a 20% and 32.7% increase in MPP power from before to after the algorithm executed for the 5×5 SP and TCT PV array, respectively. What's more, as seen in Fig. 21(c), the TCT configuration has better performance than SP configuration with a 9% improvement in MPP power.

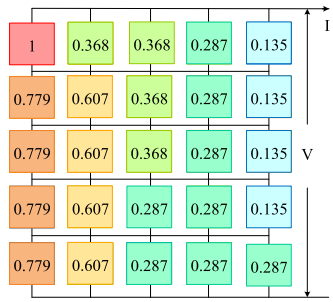

Fig. 20. Optimal configuration for a 5×5 TCT PV array.

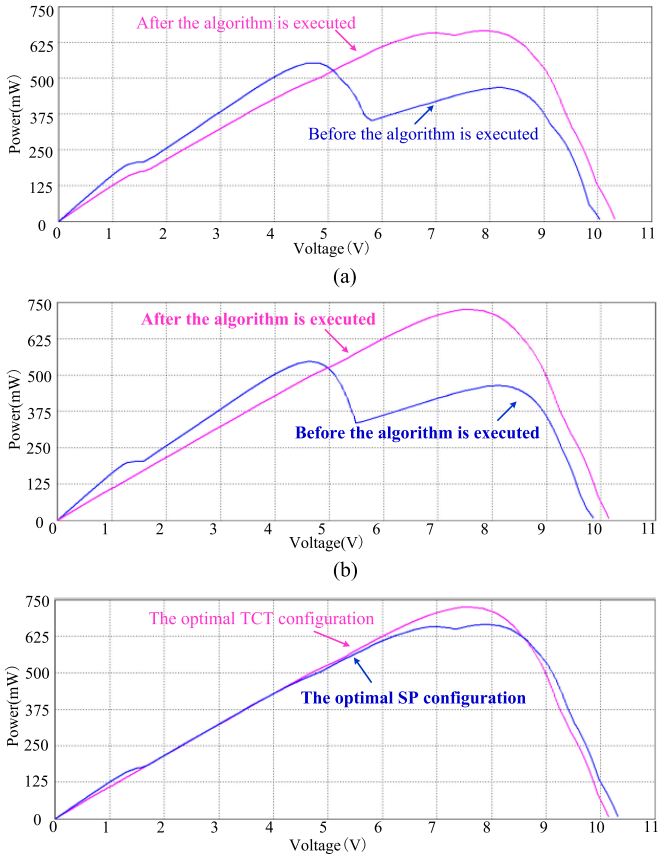

Fig. 21. Simulated $P-V$ curves of a 5×5 PV array. (a) Simulated $P-V$ curves of a 5×5 SP PV array before and after the algorithm is executed. (b) Simulated $P-V$ curves of a 5×5 TCT PV array before and after the algorithm is executed. (c) Simulated $P-V$ curves of the optimal configurations for 5×5 TCT and SP PV arrays.

IV. Experimental Results

In order to validate the results obtained in simulation, a laboratory setup was developed using 3×3 and 5×5 PV array. The insolation to these arrays is provided by the DILAS M1F4S22-808-50C-SS2.7 type high-power fiber-coupled LD module.

Fig. 22 shows the $P-V$ curves of the optimal configurations for the 3×3 SP and TCT array. As seen, the optimal TCT array achieves up to 9.2% MPP power enhancement compared with the optimal SP array. Fig. 23 shows the $P-V$ curves of the optimal configurations for the 5×5 SP and TCT array. It can be

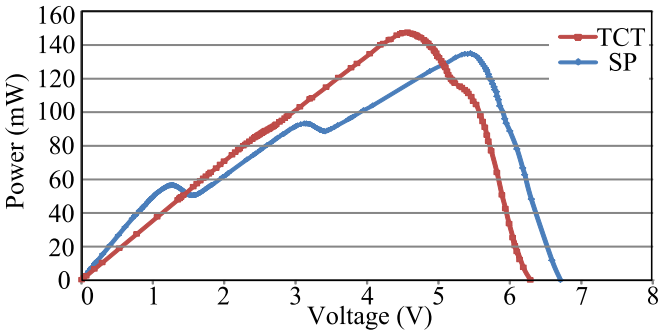

Fig. 22. $P-V$ curves of the optimal configurations for the 3×3 SP and TCT array.

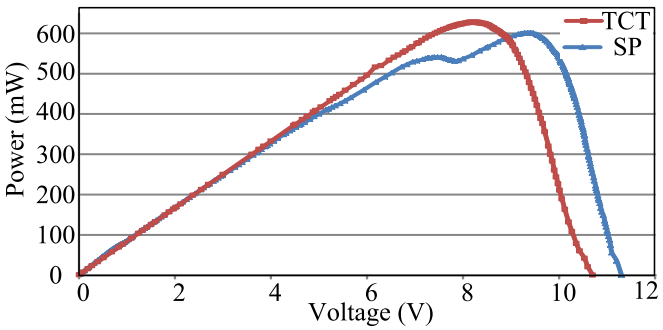

Fig. 23. $P-V$ curves of the optimal configurations for the 5×5 SP and TCT array.

seen that 4.3% MPP power level enhancement can be achieved from the optimal TCT array. The experimental results are similar to the theoretical analysis. Moreover, the $P-V$ curves of the optimal TCT array are smoother than that of SP array in these two cases, which simplifies the task of MPPT algorithm. As a consequence, the optimal TCT configuration is a good solution to cope with the Gaussian beam condition.

Moreover, in order to show the advantage of the proposed search algorithm for TCT architecture in this paper, the comparison with the algorithms in [12] and [21] is performed. Executing the algorithm, which is proposed in this paper, on a desktop computer running MATLAB, it takes 50 ms of CPU time to calculate the arrangement of a 4×4 array, while the searching time as reported in [21] for a 4×4 array using the configurations of interest computation algorithm takes 9.7 h to find the optimum. Clearly, it can be inferred that for practical situations, this will be too long to be useful. As the algorithm in [12] is based on simple comparisons and swapping, the calculation time is around 300 ns for a 4×4 array. Although this approach takes very little time to execute, the output power of the configuration, which is found by it, needs to be improved. The algorithms in this paper and [12] are executed and the corresponding optimal TCT configurations for 3×3 and 4×3 arrays are found, as shown in Figs. 24 and 25. It can be seen that the algorithm which is proposed in this paper is able to find the TCT configuration with better equalization than the algorithm in [12]. The experiment for comparing with the approachs in this paper and [12] is performed, as shown in Fig. 26. It can

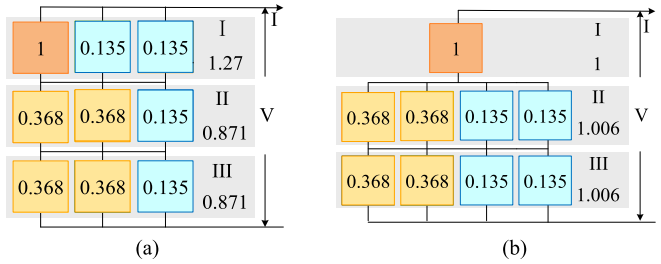

Fig. 24. Optimal configurations for a 3×3 TCT PV array found by two algorithms. (a) Optimal configuration found by the algorithm in [12]. (b) Optimal configuration found by the algorithm in this paper.

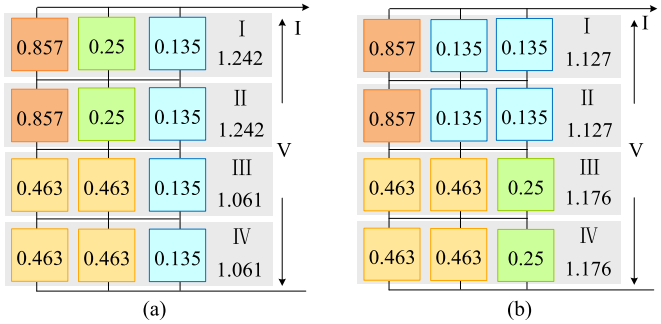

Fig. 25. Optimal configuration for a 4×3 TCT PV array found by two algorithms. (a) Optimal configuration found by the algorithm in [12]. (b) Optimal configuration found by the algorithm in this paper.

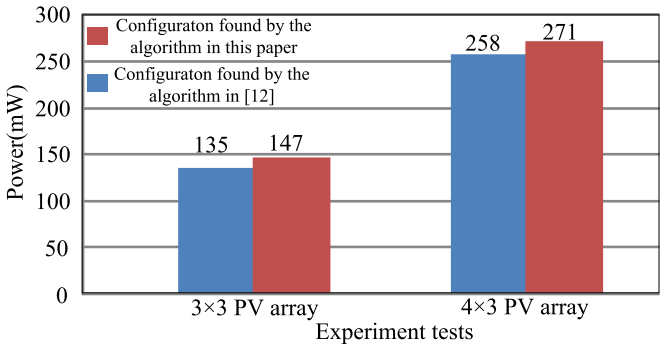

Fig. 26. Comparison of power generation between two algorithms

be seen that the proposed approach obtains an 8.1% and 4.79% output power improvement for 3×3 and 4×3 arrays, respectively. In short, it has lower requirement of the execution time for the proposed TCT configuration research algorithm since it is not designed for a dynamic array, and the execution time of it is acceptable in practice from the foregoing experiment results. Moreover, the proposed algorithm can be used to obtain a more optimal configuration compared with other algorithms.

V. Conclusion

An optimal PV array configuration search mechanism, which enhances the PV power under the Gaussian beam condition, is proposed in this paper. In order to do so, the simulated irradiance profile of the Gaussian laser beam is mathematically

modeled, which plays an important role in modeling the PV array and designing the search algorithms. The algorithms presented are designed to be compact and efficient and can be used to obtain a usable configuration for the array under Gaussian beam condition. The performances of the all available configurations for SP and TCT architectures are investigated under Gaussian beam condition, and both simulation and experimental results show that the power extracted under Gaussian beam condition is greater with the TCT configuration compared with other configurations.

REFERENCES

[1] C. S. Wang, O. H. Stielau, and G. A. Covic, "Design considerations for a contactless electric vehicle battery charger," *IEEE Trans. Ind. Electron.*, vol. 52, no. 5, pp. 1308–1314, Oct. 2005.

[2] J. Garnica, R. A. Chinga, and J. Lin, "Wireless power transmission: From far field to near field," *Proc. IEEE*, vol. 101, no. 6, pp. 1321–1331, Jun. 2013.

[3] J. T. Boys, G. A. Elliott, and G. A. Covic, "An appropriate magnetic coupling co-efficient for the design and comparison of ICPT pickups," *IEEE Trans. Power Electron.*, vol. 22, no. 1, pp. 333–335, Jan. 2007.

[4] C. S. Wang, A. C. Grant, and H. S. Oskar, "Power transfer capability and bifurcation phenomena of loosely coupled inductive power transfer systems," *IEEE Trans. Ind. Electron.*, vol. 51, no. 1, pp. 148–157, Feb. 2004.

[5] D. E. Raible, "High intensity laser power beaming for wireless power transmission," Master's thesis, Dept. Elect. Comput. Eng., Cleveland State Univ., Cleveland, OH, USA, May 2008.

[6] J. Alda, "Laser and gaussian beam propagation and transformation," *Encyclopedia of Optical Engineering*. New York, NY, USA: Marcel Dekker, 2003.

[7] H. Patel and V. Agarwal, "Maximum power point tracking scheme for PV systems operating under partially shaded conditions," *IEEE Trans. Ind. Electron.*, vol. 55, no. 4, pp. 1689–1698, Apr. 2008.

[8] A. Bidram, A. Davoudi, and R. S. Balog, "Control and circuit techniques to mitigate partial shading effects in photovoltaic arrays," *IEEE J. Photovolt.*, vol. 2, no. 4, pp. 532–546, Oct. 2012.

[9] L. Gao, R. A. Dougal, S. Liu, and A. P. Iotova, "Parallel-connected solar PV system to address partial and rapidly fluctuating shadow conditions," *IEEE Trans. Ind. Electron.*, vol. 56, no. 5, pp. 1548–1556, May 2009.

[10] P. S. Rao, G. S. Ilango, and C. Nagamani, "Maximum power from PV arrays using a fixed configuration under different shading conditions," *IEEE J. Photovolt.*, vol. 4, no. 2, pp. 679–686, Mar. 2014.

[11] L. Villa, D. Picault, B. Raison, S. Bacha, and A. Labonne, "Maximizing the power output of partially shaded photovoltaic plants through optimization of the interconnections among its modules," *IEEE J. Photovolt.*, vol. 2, no. 2, pp. 154–163, Apr. 2012.

[12] J. P. Storey, P. R. Wilson, and D. Bagnall, "Improved optimization strategy for irradiance equalization in dynamic photovoltaic arrays," *IEEE Trans. Power Electron.*, vol. 28, no. 6, pp. 2946–2956, Jun. 2013.

[13] D. Nguyen and B. Lehman, "An adaptive solar photovoltaic array using model-based reconfiguration algorithm," *IEEE Trans. Ind. Electron.*, vol. 55, no. 7, pp. 2644–2654, Jul. 2008.

[14] M. Z. Dein, M. Kazerani, and M. M. A. Salama, "Optimal photovoltaic array reconfiguration to reduce partial shading losses," *IEEE J. Sustain. Energy*, vol. 4, no. 1, pp. 145–153, Jan. 2014.

[15] Y. Wang, X. Lin, Y. Kim, N. Chang, and M. Pedram, "Architecture and control algorithms for combating partial shading in photovoltaic systems," *IEEE J. Comput.-Aided Des. Integr. Circuits Syst.*, vol. 33, no. 6, pp. 917–930, Jun. 2014.

[16] G. V. Quesada, F. G. Gispert, R. P. López, M. R. Lumbreras, and A. C. Roca, "Electrical PV array reconfiguration strategy for energy extraction improvement in grid-connected PV systems," *IEEE Trans. Ind. Electron.*, vol. 56, no. 11, pp. 4319–4331, Nov. 2009.

[17] H. Patel and V. Agarwal, "MATLAB-based modeling to study the effects of partial shading on PV array characteristics," *IEEE J. Energy Convers.*, vol. 23, no. 1, pp. 302–310, Mar. 2008.

[18] G. Walker, "Evaluating MPPT converter topologies using a MATLAB PV model," *J. Elect. Electron. Eng. Aust.*, vol. 21 no. 1, pp. 49–56, 2001.

[19] W. Lee, Y. Kim, Y. Wang, N. Chang, M. Pedram, and S. Han, "Versatile high-fidelity photovoltaic module emulation systems," in *Proc. 17th Int. Symp. Low Power Electron. Des.*, 2011, pp. 91–96.

[20] I. R. Balasubramanian, S. I. Ganesan, and N. Chilakapati. "Impact of partial shading on the output power of PV systems under partial shading conditions," *IET Power Electron*., vol. 7, no. 3, pp. 657–666, 2014.

[21] G. Velasco, J. J. Negroni, F. Guinjoan, and R. Pique. "Irradiance equalization method for output power optimization in plant oriented grid connected PV generators," presented at the Eur. Conf. Power Electronics Applications, Dresden, Germany, 2005, p. 10.

Weiyang Zhou was born in Jiangxi, China, in 1989. He received the B.S. degree in electrical engineering from the Nanjing University of Aeronautics and Astronautics, Nanjing, China, in 2011, where he is currently working toward the Ph.D. degree in electrical engineering.

His current research interests include dc–dc conversion and wireless power transfer system.

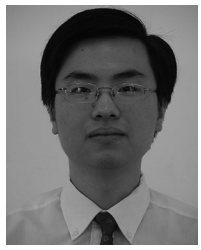

Ke Jin (S'04–M'09) was born in Nanjing, China, in 1978. He received the B.S., M.S., and Ph.D. degrees in electrical engineering from the Nanjing University of Aeronautics and Astronautics (NUAA), Nanjing, in 2000, 2003, and 2006, respectively.

From 2007 to 2008, he was a Postdoctoral Researcher with the Center for Power Electronics Systems, Virginia Polytechnic Institute and State University, Blacksburg. He is currently a Professor at the College of Automation Engineering, NUAA. He has authored more than 60 technical papers published in international journals and conference proceedings. His main research interests include high-frequency soft-switching conversion, low-voltage high-current conversion techniques, and renewable power systems.